Clays and Clay Minerals, Vol. 44, No. 3, 339–356, 1996.

CLAY-MINERAL PROVENANCE, SEDIMENT DISPERSAL PATTERNS, AND MUDROCK DIAGENESIS IN THE NANKAI ACCRETIONARY PRISM, SOUTHWEST JAPAN

MICHAEL B. UNDERWOOD[1] AND KEVIN T. PICKERING[2]

[1] Department of Geological Sciences, University of Missouri, Columbia, Missouri, 65211, U.S.A.

[2] Department of Geological Sciences, University College London, Gower Street London, WC1E 6BT, U.K.

Abstract—Offscraped strata within the toe of Nankai accretionary prism display an overall facies pattern of thickening and coarsening upward. Detrital clay minerals within the Quaternary trench-wedge facies are dominated by illite; chlorite is the second-most abundant clay mineral, followed by smectite. Relative mineral percentages change only modestly with depth. The hemipelagic clay-mineral population is virtually identical to clays washed from turbidite matrix, and different size fractions (<2 μm and 2–6 μm) show nominal amounts of mineral partitioning. Smectite content increases beneath the trench-wedge deposits, where the upper subunit of the Shikoku Basin stratigraphy (late Pliocene and early Pleistocene) includes abundance of volcanic ash. Syneruptive, subaerial chemical weathering of volcanic source rocks, together with *in situ* alteration of disseminated glass shards, caused the increase in smectite. Smectite begins a monotonic transformation to illite/smectite (I/S) mixed-layer clay at ~555 mbsf and an estimated temperature of ~65 °C. Ordered (R = 1) I/S interlayering first appears at ~1220 mbsf (<2 μm size fraction) and ~1100 mbsf (<0.2 μm size fraction). The illitization gradient coincides with a reduction in pore-water chlorinity, but depth-related changes in bulk mudstone geochemistry (K_2O, Rb) are subtle. The absolute abundances of discrete smectite and I/S appear to be insufficient to account for the magnitude of pore-water dilution via *in situ* dehydration reactions. Instead, pore water probably was transported to Site 808, either from sources located deeper in the accretionary prism, where bulk mudstone porosities are lower, or from strike-parallel sources where mudstones originally deposited in the Shikoku Basin might contain higher percentages of smectite.

Key Words—Clay mineralogy, Diagenesis, Mixed-layer illite/smectite, Mudrock geochemistry, Nankai Trough, Shikoku Basin.

INTRODUCTION

The Nankai Trough region off the southwest coast of Japan (Figure 1) is one of the most thoroughly studied sites of late Cenozoic trench sedimentation and accretionary-prism tectonics (Boggs 1984; Le Pichon et al. 1987a, 1987b; Okuda and Honza 1988; Moore et al. 1990). Four legs of the DSDP (Deep Sea Drilling Project) and ODP (Ocean Drilling Program) have been completed for this area (Karig et al. 1975; Klein et al. 1980; Kagami et al. 1986; Taira et al. 1991). Relative to other subduction margins, such as Barbados (Moore et al. 1988) and the nearby Japan Trench (von Huene and Arthur 1982; Cadet et al. 1987), the flux of terrigenous sediment to the Nankai Trough is high. Therefore, the stratigraphy of the accretionary prism serves as an effective modern analogue for uplifted sandstone-rich accreted terranes such as the Franciscan Complex of California (Blake et al. 1985), the Kodiak Islands of Alaska (Moore et al. 1983) and the Shimanto Belt of Japan (Taira et al. 1988).

ODP Leg 131 was designed to investigate structural fabrics, physical properties and aqueous geochemistry within the toe of the Nankai accretionary prism (Taira et al. 1992). Excellent core recovery also allowed us to document stratigraphic and sedimentary-facies relations in unprecedented detail (Figure 2). Several aspects of Site 808 merit special consideration. First, the holes were spudded on the landward trench slope less than 150 m above the thalweg of the present-day trench. A fixed reference point on the subducting oceanic basement, located immediately beneath Site 808, first entered the trench environment at about 0.46 Ma. At that time, Miocene to early Quaternary abyssal-plain deposits of the Shikoku Basin were buried rapidly beneath a landward-thickening wedge of terrigenous turbidites. Frontal accretion by imbricate thrusting has transferred material above the décollement into the prism toe. A carapace of lower slope deposits (roughly 20 m) caps the accreted succession (Figure 2). Whereas previous DSDP drill sites were located farther down the axial gradient and closer to the western edge of the trench, Site 808 was drilled near the center of the basin (Figure 1), along the trend of an extinct back-arc spreading center that formed the oceanic lithosphere of Shikoku Basin (Chamot-Rooke et al. 1987; Le Pichon et al. 1987a). Basement relief has been buried by the trench wedge, but the inherited bathymetric high clearly affected local rates of sedimentation (Pickering et al. 1993a). One reason for selecting the site was because total sediment thickness is at a regional minimum, which allowed penetration

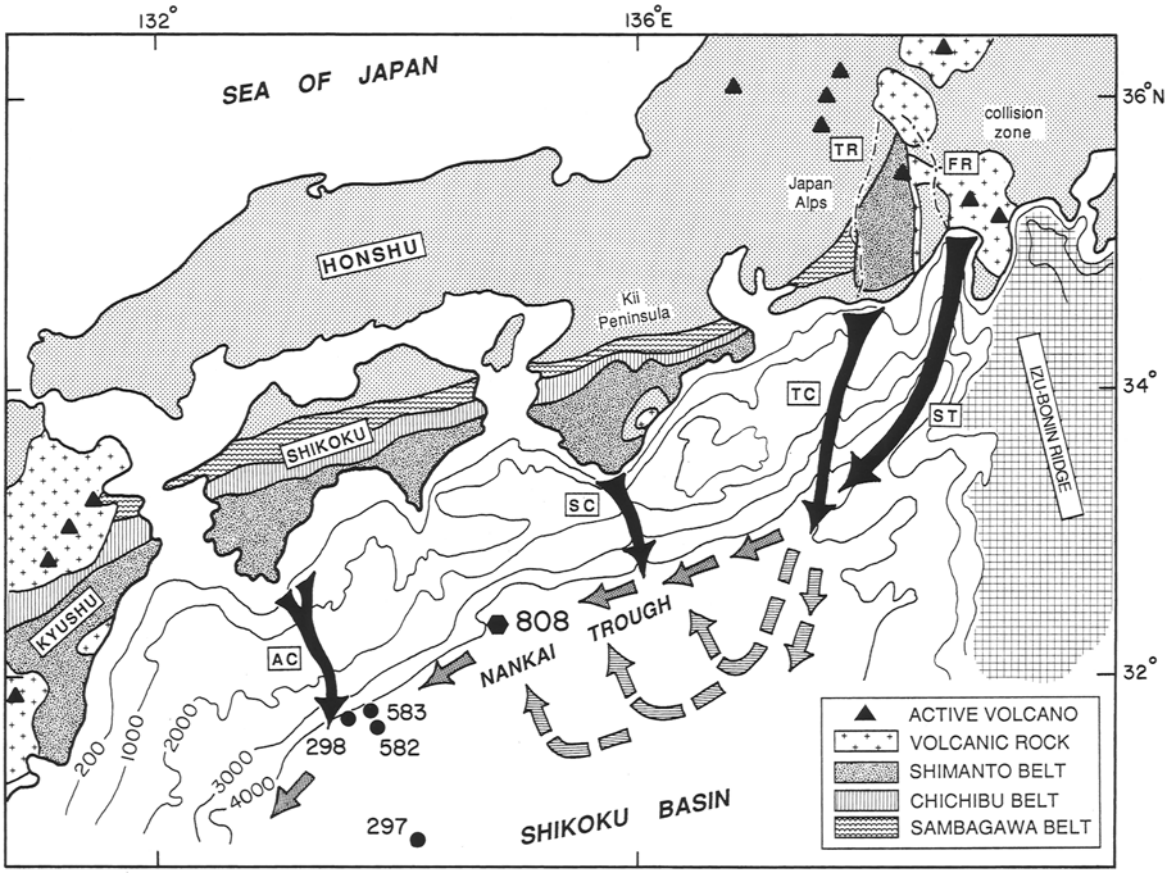

Figure 1. Index map showing the regional geography, geology and bathymetry (in meters) of the Nankai study area of southwest Japan. Numbers refer to DSDP and ODP site localities. Large black arrows symbolize major submarine canyons. Key: ST = Suruga Trough; TC = Tenryu Canyon; SC = Shino-misaki Canyon; AC = Ashizuri Canyon. Smaller arrows represent inferred pathways for turbidity currents within the trench, including flow-reflection trajectories off the seaward slope (Pickering et al. 1992; Underwood et al. 1993a). Major drainage basins in the Izu-Honshu collision zone include the Tenryu River (TR) and the Fuji River (FR).

through the décollement and into igneous basement at a depth of only 1290 meters below seafloor (mbsf). Finally, because the subducting lithosphere is young (spreading ceased approximately 15 Ma) and the drill site is located near the extinct spreading axis, heat flow is unusually high for an accretionary prism (Yamano et al. 1984). The average geothermal gradient recorded at Site 808 is approximately 110 °C/km (Shipboard Scientific Party 1991; Yamano et al. 1992) and this thermal regime has exerted considerable influence on sediment diagenesis, particularly at depths below about 600 mbsf.

Details of our shorebased investigations have been presented elsewhere (Underwood et al. 1993a, 1993b; Pickering et al. 1993a, 1993b). The purposes of this paper are: 1) to review the mineralogic and geochemical evidence for interpretations of detrital provenance and regional sediment dispersal within Nankai Trough; 2) to summarize the mineralogic and geochemical trends associated with early sediment diagenesis; and 3) to evaluate whether or not *in situ* smectite-to-illite conversion has affected the fluid budget of the prism toe.

GEOLOGIC BACKGROUND

Lithofacies Trends

Previous drilling through the toe of the Nankai accretionary prism (Sites 298 and 583) and through the floor of Nankai Trough (Site 582) demonstrated that the trench fill is dominated by sand turbidites, with interlayers of hemipelagic mud (Moore and Karig 1976; Coulbourn 1986). The sedimentary succession recovered at Site 808 displays an overall mega-cycle of coarsening and thickening upward (Figure 2), which is consistent with the conventional paradigm of convergent-margin sedimentation (Piper et al. 1973; Schweller and Kulm 1978). Rates of sediment accumulation for the trench-wedge facies (Unit II) range from approximately 785 m/m.y. to 1380 m/m.y. (Ship-

https://doi.org/10.1346/CCMN.1996.0440304 Published online by Cambridge University Press

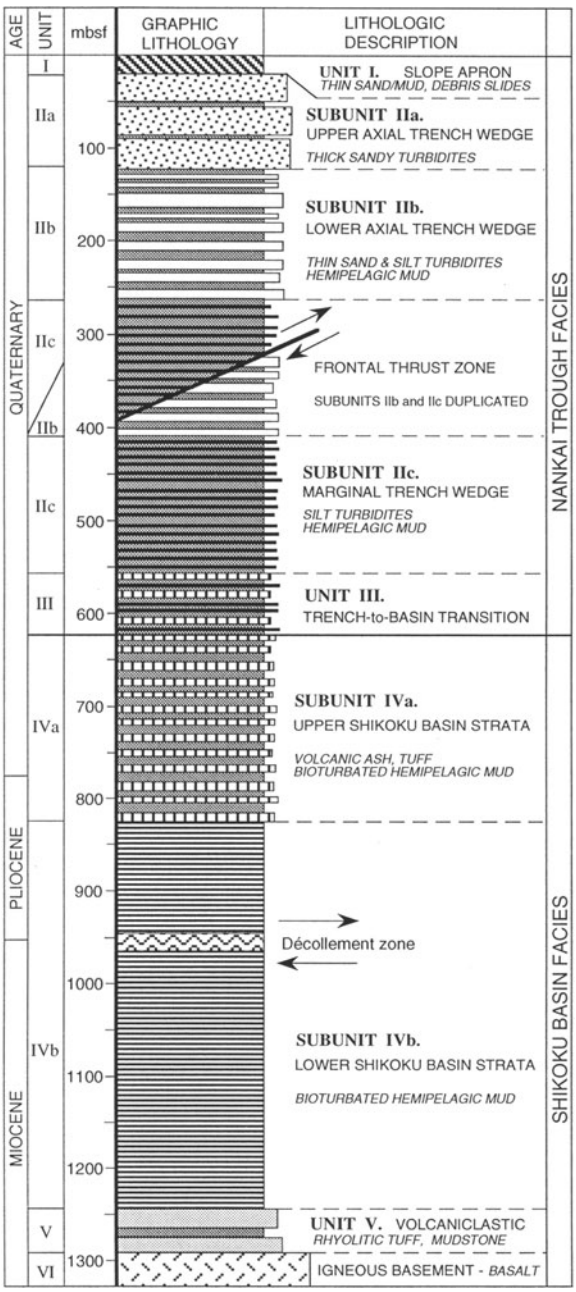

Figure 2. Stratigraphic column for ODP Site 808. Modified from Shipboard Scientific Party (1991).

board Scientific Party 1991). Outer trench-wedge sediments coincide with the first appearance (moving upsection) of silty terrigenous turbidites at 620 mbsf (Figure 2). Rates of sediment accumulation for the hemipelagic Shikoku Basin deposits (Unit IV) range from approximately 5 m/m.y. to 215 m/m.y. (Shipboard Scientific Party 1991). The upper subunit (IVa) contains abundant volcanic ash layers, whereas the lower subunit (IVb) is devoid of volcaniclastic material (Figure 2). A transitional facies (Unit III) displays characteristics of both the outer marginal trench wedge of silty turbidites and the upper part of the Shikoku Basin section of mud and ash layers. The décollement zone at the base of the accretionary prism occurs at 945–964 mbsf, within the middle of subunit IVb. The oldest strata above subducting basement (Unit V) contain thick layers of graded and cross-stratified rhyolitic tuff interbedded with variegated hemipelagic mudstone and pelagic claystone of middle Miocene age (13.6 Ma). The top of basaltic basement was encountered at approximately 1290 mbsf (Figure 2).

Sediment Provenance

Several present-day bathymetric features need to be considered for the Nankai Trough region, particularly as they relate to sediment dispersal via gravity flow. The northeast end of the trench is connected directly to a major sediment conduit, Suruga Trough (Le Pichon et al. 1987b; Nakamura et al. 1987). This canyon system begins near the shoreline with many small channels and slope gullies of the Fuji River fan-delta (Figure 1). Nankai deep-sea channel emanates from the mouth of Suruga Trough and continues down the axial gradient of the trench for a distance of at least 400 km (Shimamura 1989). Three other large submarine canyons are incised into the landward trench slope (Tenryu, Shiono-misaki and Ashizuri). Fan-shaped sediment bodies occur at the mouths of Tenryu and Shiono-misaki canyons (Le Pichon et al. 1987b; Shimamura 1989; Soh et al. 1991), so there must be local transverse input into the trench in addition to axial flow of turbidity currents. Ripple cross-laminae show that many of the turbidity currents were deflected off the seaward trench slope before continuing down the southwest-directed axial gradient (Pickering et al. 1992).

Petrographic analyses of turbidite sands associated with the Nankai Trough have led to the conclusion that most of the coarse-grained detritus was funneled initially through Suruga Trough (Figure 1) before moving southwest down the axial trench gradient (Taira and Niitsuma 1986; De Rosa et al. 1986; Marsaglia et al. 1992; Underwood et al. 1993a). The turbidite sands at Site 808 contain a wide variety of neovolcanic and paleovolcanic fragments, with lathwork, microlitic, felsitic and vitric textures, in addition to sedimentary-rock fragments consisting primarily of shale and mudstone, fresh euhedral plagioclase, both monocrystalline and polycrystalline quartz (chert) and minor amounts of low-grade metamorphic-rock fragments. This detritus matches the subaerial geology of the Izu-Honshu collision zone (Figure 1), as summarized by Ogawa et al. (1985), Ogawa and Taniguchi (1988), Toriumi and Arai (1989) and Soh et al. (1991). Lithologies are diverse and include the following fundamental units: accreted sedimentary and volcanic rocks of the Shimanto

https://doi.org/10.1346/CCMN.1996.0440304 Published online by Cambridge University Press

Belt; ophiolitic rocks of early Tertiary age; Neogene sedimentary rocks composed of fine-grained tuffaceous and terrigenous debris; quartz diorite bodies that intruded the Miocene volcaniclastic units; and Quaternary volcanic centers (including Mt. Fuji). Burial metamorphism within the collision zone ranges from the zeolite facies to prehnite-pumpellyite facies and actinolite-greenschist facies (Toriumi and Arai 1989). Superimposed on the regional pattern of burial metamorphism are zones of contact metamorphism associated with the Miocene intrusions; metamorphic grades within the contact aureoles are as high as amphibolite facies (Toriumi and Arai 1989). Simultaneous volcanism and rapid uplift of accreted rocks during collision are responsible for a mixed detrital-provenance signature.

Clay minerals from the Nankai Trough (Sites 298, 582 and 583) and Shikoku Basin (Sites 297, 442, 443 and 444) were analyzed previously by Cook et al. (1975), Chamley (1980) and Chamley et al. (1986). Within the Pleistocene turbidite section, Chamley et al. (1986) documented a predominance of illite and chlorite and suggested that most of the sediments were fed axially from sources located near the Izu Peninsula of central Japan. This is from the same source as the turbidite sand. Smectite and mixed-layer clays increase in abundance down-section in the Shikoku Basin.

Porewater Geochemistry

Shipboard analyses of interstitial water chemistry during Leg 131 led to several important observations regarding the hydrogeology of the central Nankai accretionary prism (Shipboard Scientific Party 1991). First, there is a pronounced reduction in chloride concentrations below about 570 mbsf, and the lowest concentrations occur below the décollement zone at 1040 to 1080 mbsf. Gradual changes in concentration gradients of most dissolved chemical constituents occur between 400 and 600 mbsf. These changes coincide with the lithologic transition from the marginal trench-wedge facies (subunit IIc) into interlayered ash deposits and mudstones of the Shikoku Basin (subunit IVa). Changes for some aqueous constituents, particularly an increase of H_4SiO_4, but also Ca, Mg and SO_4, also occur at the lithologic boundary near 820 mbsf (contact between subunits IVa and IVb). Finally, stratigraphic intervals with abundant layers of volcanic ash (560–820 mbsf) show large variations in dissolved silica concentrations, together with more subtle anomalies in dissolved calcium, lithium and strontium. Collectively, the porewater data demonstrate that sediment diagenesis and fluid-sediment exchange have occurred within the accretionary prism (Gieskes et al. 1993; Kastner et al. 1993). It is important to evaluate how specific clay minerals have influenced this hydrogeochemical budget.

Geothermal Regime

Many subduction zones are characterized by relatively low geothermal gradients due to the subduction of old oceanic lithosphere (Yamano et al. 1982). Under such circumstances, documentation of important diagenetic reactions is impeded because favorable temperature conditions occur beyond the depth limits of conventional DSDP and ODP boreholes. The Nankai Trough is a region of high heat flow because the subducting Shikoku Basin lithosphere is relatively young (Yamano et al. 1984; Ashi and Taira 1993). The last phase of volcanic activity in the Shikoku Basin was spatially disorganized and ended about 12 Ma (Chamot-Rooke et al. 1987). The present-day heat flow at Site 808 is equal to approximately 130 mW/m^2, and the average linear geothermal gradient within the upper 350 m of the accretionary prism is ~110 °C/km (Shipboard Scientific Party 1991; Yamano et al. 1992). Thus, Site 808 is ideally suited for studies of early sediment diagenesis at relatively shallow depths.

METHODS

Details of laboratory methodology have been described by Underwood et al. (1993a, 1993b) and Pickering et al. (1993a, 1993b). In brief, X-ray fluorescence (XRF) spectrometry was used to detect concentrations of major element oxides (weight-%), together with selected minor and trace elements (ppm). All of the geochemical data presented here come from analyses of bulk mud and mudstone samples. Clay minerals were analyzed using a Scintag PAD V system interfaced with a Microvax 2000 microprocessor. Oriented aggregates of the 2 to 6 μm and <2 μm size fractions were prepared by vacuum-filtration and filter-peel transfer, then saturated with ethylene glycol. Digital output was processed through a background correction and a deconvolution program designed to fit peaks to a Split Pearson VII profile shape (Gaussian-Lorentzian hybrid). Relative weight percentages of the dominant clay minerals are based on peak areas of the smectite (001), illite (001) and the composite chlorite (002) + kaolinite (001) reflections (Figure 3). Representative samples were boiled in HCl and analyzed a second time to establish the approximate amount of kaolinite (Starkey et al. 1984).

Most data sets that describe clay-mineral abundances for marine sediments are based on the Biscaye (1965) weighting factors (McManus 1991). We conducted tests of accuracy using measured weight percentages of chlorite, illite and smectite standards obtained from the Clay Mineral Society Repository, and the error is as high as 20% (Underwood et al. 1993a). The following weighting factors were then calculated algebraically from the mineral-standard data, and they reduce the maximum error to approximately 10% and the average error to less than 5%: smectite (001) =

https://doi.org/10.1346/CCMN.1996.0440304 Published online by Cambridge University Press

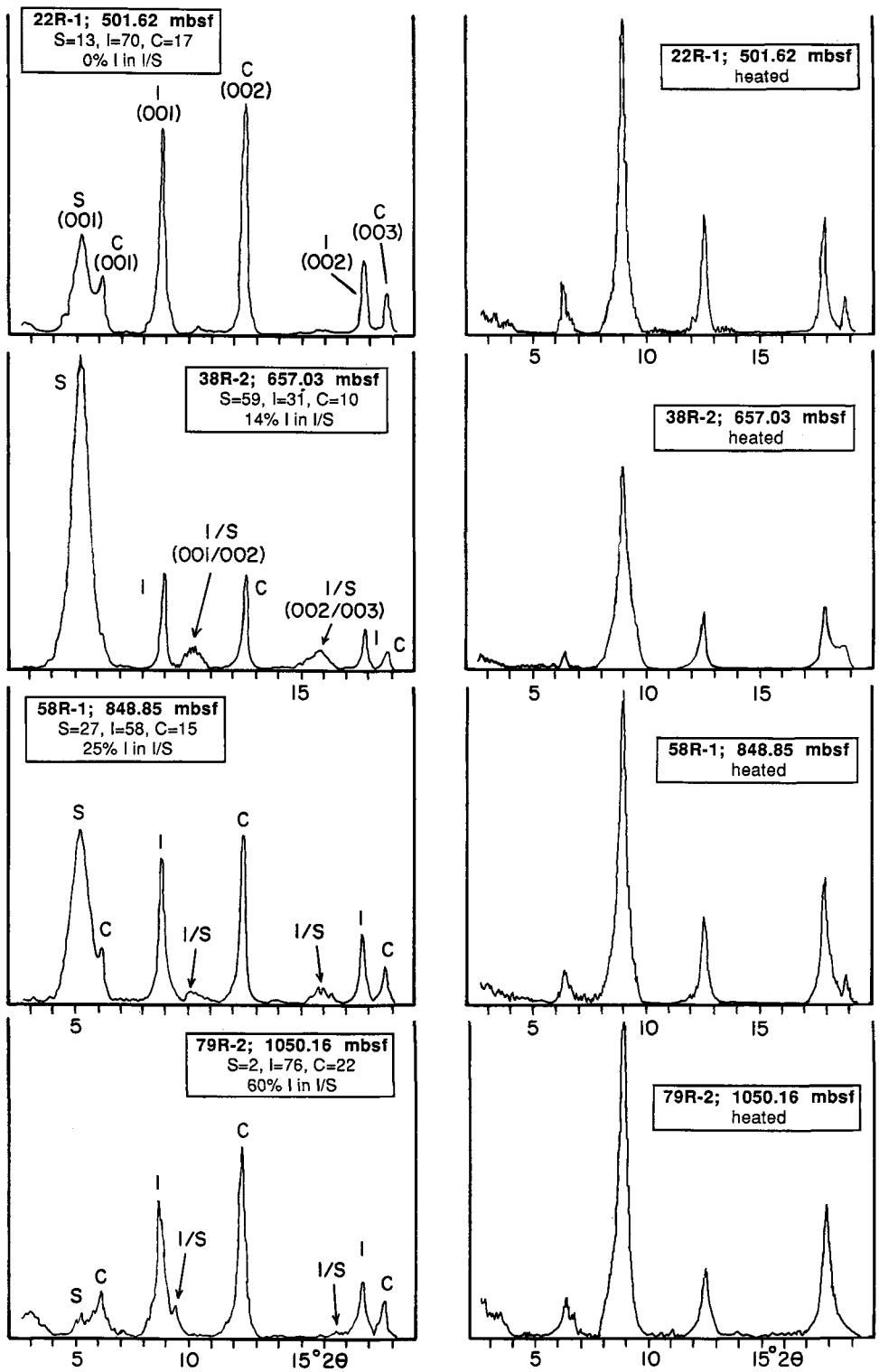

Figure 3. Representative examples of X-ray diffractograms, plotted after background correction of digital data, showing peaks used to calculate clay-mineral percentages and illite content of I/S mixed-layer clays. Examples to the left are for specimens saturated with ethylene glycol; examples on the right are for the same specimens following heating to 375 °C. See Underwood et al. (1993a) for a complete discussion of peak-area weighting factors and error analysis.

https://doi.org/10.1346/CCMN.1996.0440304 Published online by Cambridge University Press

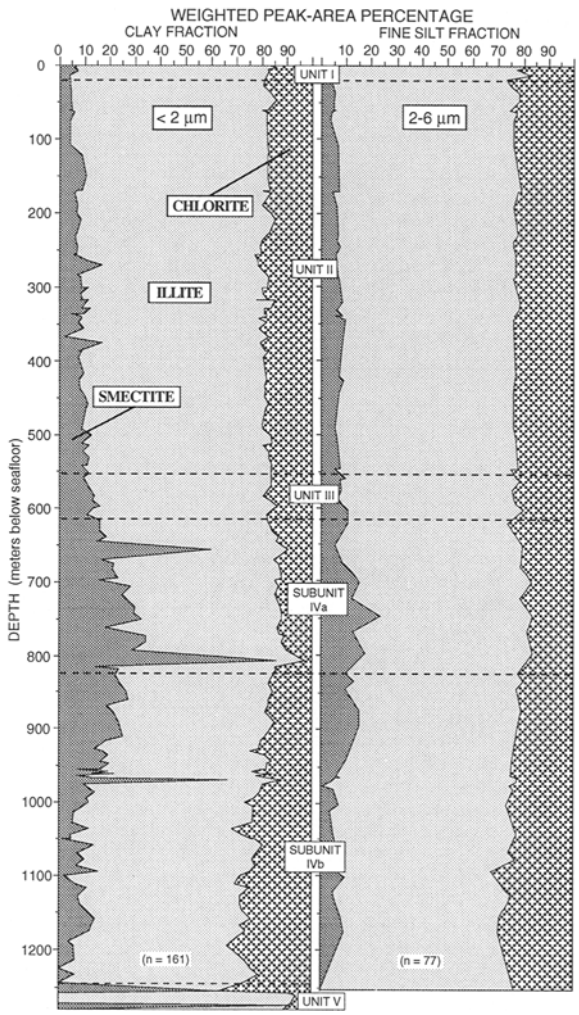

Figure 4. Relative percentages of smectite, illite and chlorite+kaolinite at Site 808, based on integrated peak areas (glycolated) and weighting factors of Underwood et al. (1993a). Separate analyses were completed for the <2 μm and 2 to 6 μm size fractions. Underwood et al. (1993a, 1993b) offers complete listings of data, including recalculations based on the peak-area weighting factors of Biscaye (1965).

1X; illite (001) = 8X; and chlorite (002) + kaolinite (001) = 1.8X. In reality, all correction factors change with the absolute abundance of each clay mineral, impurities in the mineral standards, variations in illite crystallinity and smectite chemistry, and peak broadening caused by interference from I/S. We did not attempt to estimate the relative percentages of I/S mixed-layer clay with respect to the total clay-mineral population. Small amounts of mixed-layer clay probably have been recorded in the counts used to estimate both %-illite and %-smectite. Therefore, our data remain semi-quantitative.

Several methods exist to calculate the ratios of illite and smectite crystallites in mixed-layer phases (Reynolds and Hower 1970; Srodon 1980, 1981; Inoue et al. 1989), but many are inappropriate if samples contain abundant discrete illite. As shown in Figure 3, we determined the angular separation (Δ °2θ) between the composite illite-(001)/smectite-(002) reflection (at ~9 to 10 °2θ) and the composite illite-(002)/smectite-(003) reflection (at ~16 to 17 °2θ) and utilized a mixing equation calculated from the data summarized by Moore and Reynolds (1989). Hathon (1992) showed that abundances of illite and smectite layers determined this way are between 2% and 8% of values based on visual counts of TEM images. Most of the peak intensities generated by the composite (001/002) and (002/003) peaks are quite subdued (Figure 3). The 0.2 μm size fraction from thirteen representative samples was also analyzed to confirm the results. In addition, representative samples were analyzed under three different conditions (air-dried, glycol-saturated and heated to 375 °C) to make sure that the low-intensity peaks in question conformed to the expected behavior, as summarized by Moore and Reynolds (1989).

RESULTS

Composition of the Trench Wedge

Relative percentages of smectite, illite and chlorite(+kaolinite) for the entire stratigraphic column at Site 808 are shown in Figure 4. The clay mineralogy of hemipelagic deposits is quite uniform within the upper 600 m of the stratigraphic section. Detrital illite is clearly the most abundant constituent (average = 73%), followed by undifferentiated chlorite + kaolinite (average = 18%), then discrete smectite. Chlorite accounts for 92 to 80% of the composite 7 Å peak area (average equals 86%). Therefore, the kaolinite content probably amounts to no more than about 3% of the total clay-mineral population. There is only a modest amount of mineral partitioning as a function of grain size. The most obvious difference is a consistent enrichment of chlorite within the larger size fraction. Conversely, smectite content increases in the <2 μm fraction, particularly at depths below 480 mbsf (Figure 4). Figure 5 shows a comparison among clay-mineral percentages and the type of host sediment within the trench-wedge facies. With few exceptions, there are only minor differences between the background lithology of hemipelagic mud and clay-sized matrix washed from turbidite interbeds. These differences fall within the brackets of analytical error. We conclude that the turbidites and hemipelagites contain the same population of clay minerals eroded from the same general area of the Japanese Islands.

Because detrital illites are the dominant clays within both hemipelagic and turbidite deposits, we characterized those minerals in greater detail (Underwood et al. 1993a). Most values of illite crystallinity index (<2 μm size fraction) fall within the zone of anchimeta-

https://doi.org/10.1346/CCMN.1996.0440304 Published online by Cambridge University Press

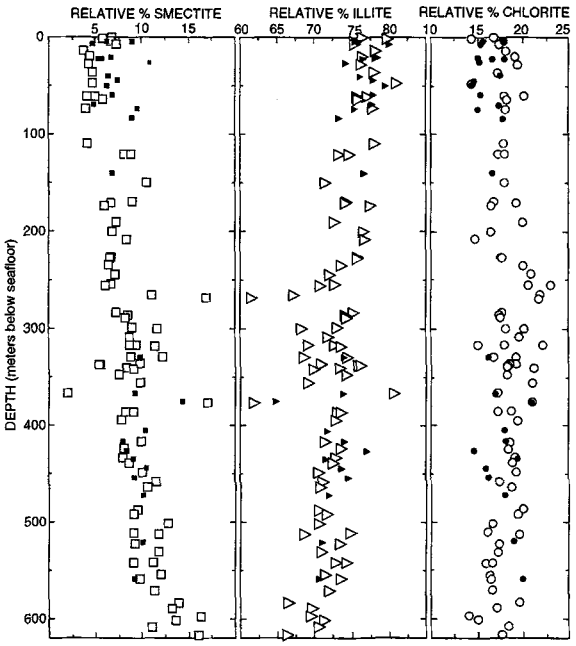

Figure 5. Comparison of relative clay-mineral percentages (<2 μm size fraction) for hemipelagic muds (open symbols) and turbidite matrix (closed symbols) at Site 808. Values are based on weighting factors of Underwood et al. (1993a).

morphism (incipient greenchist facies). In addition, the $2M_1$ variety of illite is the most abundant polytype. Values of b_0 are consistent with low phengite contents and source terranes subjected to intermediate P-T gradients.

Clay Diagenesis

The biggest challenge in interpreting mineralogic changes down-section at Site 808 is to separate the temporal effects of changing detrital provenance from the depth-dependent effects of diagenetic alteration. Sediments within the Nankai trench-wedge facies accumulated at exceptionally rapid rates of approximately 1380–785 m/m.y. (Shipboard Scientific Party 1991). Conversely, sediment accumulation rates calculated for the Shikoku Basin hemipelagic deposits (below the base of Unit III) drop off significantly, with most values between 125 m/m.y. and 10 m/m.y. This change in the overall style of sedimentation reflects the dramatic difference between the turbidite-dominated trench wedge and the slow fall-out of suspended sediment onto the floor of the Shikoku Basin. In addition, the youngest subunit of the Shikoku Basin is enriched with discrete layers of volcanic ash and lithified tuff. Significantly, this facies transition coincides with a shift in clay mineralogy, as defined by slight increases in the content of smectite (Figure 4).

The gradual enrichment of smectite, which actually begins at the top of Unit III, is much more obvious for the <2 μm size fraction, as compared to the 2 to 6 μm size split (Figure 4). Maximum background values of 30 to 35% smectite occur at a stratigraphic position of ~800 mbsf. Superimposed on this trend are local spikes in %-smectite (up to 70% to 90%) that mark the presence of possible bentonite layers. These mudstones do not display any obvious differences in texture or color. The spot occurrences of bentonites within homogeneous bioturbated mudstones leads us to suspect that other smectite-rich intervals remain undetected. The monotonic increase in smectite within Unit IV correlates well with XRD evidence for diagenetic alteration of discrete ash layers (Masuda et al. 1993). Furthermore, the increase in authigenic smectite coincides with the occurrence of a zeolite mineral (clinoptilolite), which is a common replacement product of siliceous volcanic glass (Shipboard Scientific Party 1991). Below a depth of approximately 820 mbsf, the smectite content drops off steadily to the base of subunit IVb. Unlike other subduction zones, such as Barbados (Tribble 1990; Vrolijk 1990), there are no clay-mineral anomalies associated with the décollement zone (945 to 964 mbsf). Finally, clay-mineral abundances within the volcaniclastic succession of Unit V are very erratic (Figure 4), which depends upon whether specimens are from rhyolitic tuff layers (smectite spikes) or from variegated interbeds of hemipelagic mudstone (illite-rich).

Composite (001/002) and (002/003) peaks produced by disordered (R = 0) mixed-layer clays were first detected above the background noise for the <2 μm size fraction at a sample depth of 555 mbsf. There is a monotonic increase in the proportion of illite in I/S through the remainder of the stratigraphic section (Figure 6). At the lithologic boundary between subunits IVa and IVb (820 mbsf), there is about 25% to 30% illite in the I/S. The maximum amount of interlayered illite (78%) occurs at a depth of approximately 1220 mbsf (Figure 6). The development of a regular 1:1 stacking arrangement of I/S interlayers produces a robust second-order superstructure reflection (002*) at a diffraction angle of approximately 6.5 °2θ. We detected this Reichweite = 1 (R = 1) ordering beginning at a depth of 1223 mbsf in the <2 μm size fraction. R = 1 ordering occurs at a shallower depth of approximately 1100 mbsf in the <0.2 μm size fraction (Figure 6). This increase in the illite component of I/S clays probably contributed to the reduction of detrital and volcanogenic smectite within subunit IVb (Figure 4).

Major Element Geochemistry of Mudrocks

The bulk chemical compositions of sediments from Site 808 are remarkably uniform throughout most of the section (Pickering et al. 1993b). The average oxide percentages, which are uncorrected for ignition loss, are: SiO_2 = 64.31; Al_2O_3 = 16.12; Fe_{total} = 6.25; MnO = 0.40; MgO = 2.50; CaO = 3.28; Na_2O = 2.68; K_2O = 3.04; TiO_2 = 0.70; and P_2O_5 = 0.30. Silica concen-

https://doi.org/10.1346/CCMN.1996.0440304 Published online by Cambridge University Press

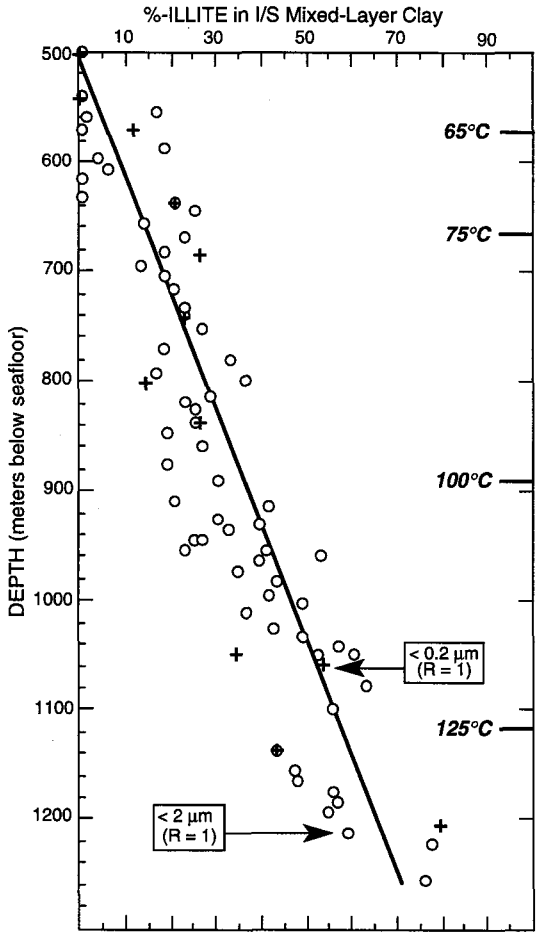

Figure 6. Estimates of percent illite in I/S mixed-layer clays at Site 808. Symbols denote two groups of size fractions: <2 µm (open circles) and <0.2 µm (crosses). Calculations are based on the angular separation between the composite illite (001)/smectite (002) peak at 9.0°–10.3 °2θ and the illite (002)/smectite (003) peak at 15.8°–17.4 °2θ (Figure 3). Temperature estimates are based on linear projections of a borehole gradient of 110 °C/km (Shipboard Scientific Party 1991).

trations for background mudstones at Site 808 typically range from 62 to 69%, and the average SiO_2/Al_2O_3 ratio is approximately 4.0. Trench-fill turbidites are slightly enriched with SiO_2 relative to the mudstones deposited in Shikoku Basin (Figure 7). When normalized to Al_2O_3, there are no systematic changes in major elements as a function of depth or stratigraphic age, nor did we detect any dramatic differences between the compositions of the trench-wedge deposits and those of the underlying hemipelagites of the Shikoku Basin. There are slight decreases in SiO_2/Al_2O_3 and TiO_2/Al_2O_3 within the Shikoku Basin facies (Figure 7). The most obvious departure from the geochemical background occurs at approximately 1100 mbsf, where there are sharp spikes for total-iron/alumina, MnO/Al_2O_3 and CaO/Al_2O_3 ratios, together with a more subdued increase for the MgO/Al_2O_3 ratios. Cores within this depth interval (1087–1111 mbsf) display varicolored bands and diffuse laminae, irregular patches of diagenetic carbonate and siderate nodules (Shipboard Scientific Party 1991). Analyses of trace elements show dramatic increases for Ba, Y, Sr, La and Ce within this interval (Pickering et al. 1993b). The geochemical anomaly was attributed to hydrothermal alteration (Pickering et al. 1993b; Underwood et al. 1993b), although the timing of the event remains unknown. Significant oscillations for the major-oxide ratios also occur within Unit V. These variations are associated with differences between rhyolitic tuff layers and claystone interbeds (Figure 8).

The typical mudrock geochemistry for Site 808 compares favorably with data from the Leg 31 and 87 drill sites (Donnelly 1980; Kawahata et al. 1986; Minai et al. 1986). We agree with Minai et al. (1986), who suggested that slight variations in silica concentration at Sites 582 and 583 are due to fluctuations in bulk mineral composition and grain-size distribution. A large component of the total silica budget, particularly within the trench-wedge facies, probably is tied up in silt-sized detrital quartz, feldspar and lithic fragments. Shipboard XRD analyses of bulk powders indicate that the detrital silt components constitute up to 70–80% of the bulk mud (Shipboard Scientific Party 1991).

Because of the preponderance of detrital silt, chemical effects of clay-mineral diagenesis are subtle. Beginning at 800 mbsf, absolute values of K_2O increase from about 2.9% to 3.8%, and the concentration of Rb increases from approximately 110 to 160 ppm (Figure 9). The start of this geochemical trend matches the depth zone in which dissolved potassium from pore waters decreases to minimum values (Figure 9) and the percentage of illite in I/S increases from ~20% to ~60% (Figure 6). We suggest that the chemical changes were caused by uptake of K and Rb cations by authigenic illite.

DISCUSSION

Trench-wedge Provenance

The stratigraphic uniformity and close correspondence between the respective clay mineralogies of hemipelagic muds and turbidite matrix in the Nankai trench-wedge facies may not be surprising. However, the background fallout of suspended sediment does not always follow the same pattern of regional-scale sediment dispersal as transport by turbidity currents (Underwood 1986, 1991; Hathon and Underwood 1991). Repeated episodes of mud resuspension and mineral homogenization are common within the near-bottom nepheloid layer in response to bioturbation, thermohaline bottom currents and turbidity currents (Gorsline 1984, 1985). In contrast, discrete turbidite deposits are more likely to show irregular variations and/or ex-

https://doi.org/10.1346/CCMN.1996.0440304 Published online by Cambridge University Press

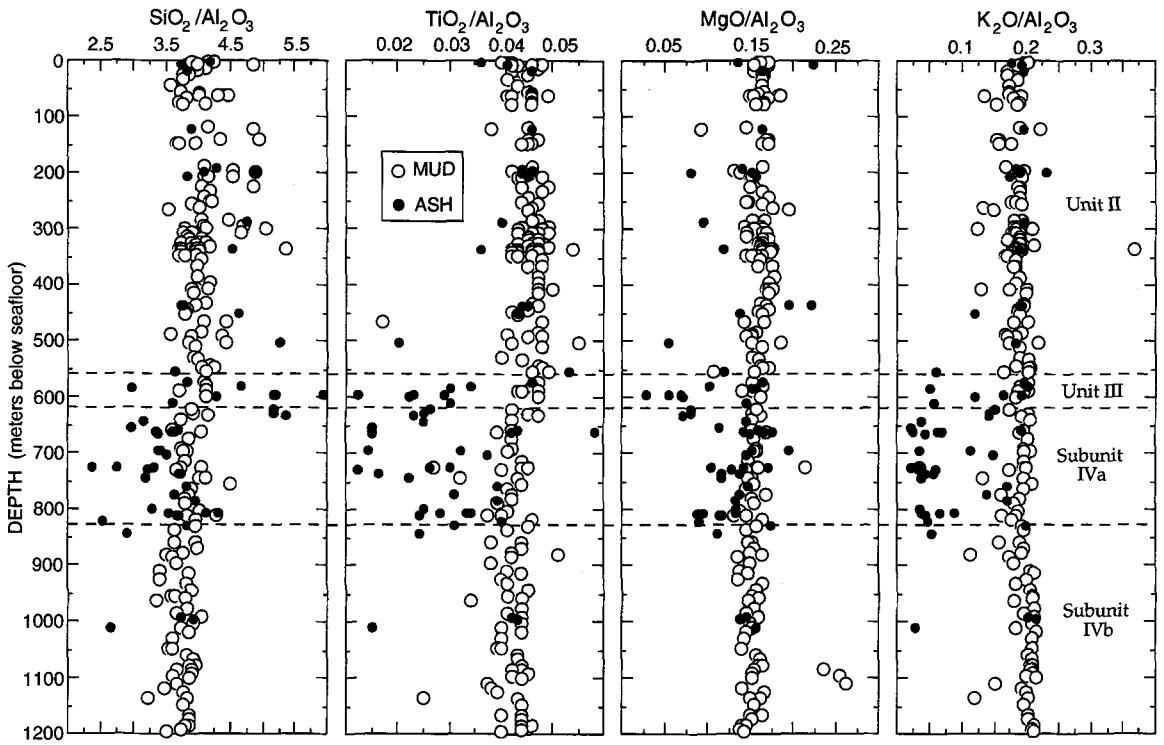

Figure 7. Comparisons among major-element oxide ratios for bulk samples of mud and mudstone (open circles) versus interbeds of ash and tuff (solid dots) at Site 808. Results from Unit V are shown in Figure 8. Pickering et al. (1993b) and Masuda et al. (1993) offer complete listings of data.

treme spikes for detrital sand modes, particularly if they are derived from multiple and diverse sources (Underwood and Norville 1986). The uniform nature of clay minerals in the trench interbeds at Site 808 leads us to believe that a single source region has been dominant throughout their accumulation. Although some of this mineralogic homogeneity could be caused by clay infiltration following deposition of the coarser grained sand layers, the infiltration mechanism seems less plausible for layers of turbidite silt with lower permeabilities. The turbiditic clay minerals probably occupied interstitial spaces in the suspended cloud during the stages of transport, gravitational collapse and deposition. We conclude that the clay minerals

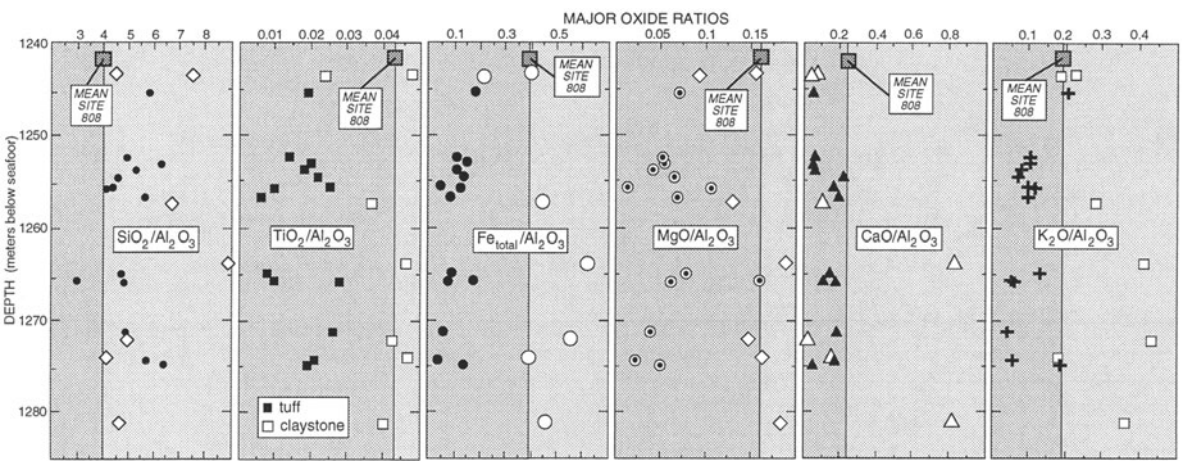

Figure 8. Comparisons among major-element oxide ratios for Unit V at Site 808. Geochemical domains are plotted relative to average ratios for Site 808. Solid symbols correspond to tuff samples; open symbols denote bulk samples of variegated claystone. Pickering et al. (1993b) and Masuda et al. (1993) offer complete listings of data.

https://doi.org/10.1346/CCMN.1996.0440304 Published online by Cambridge University Press

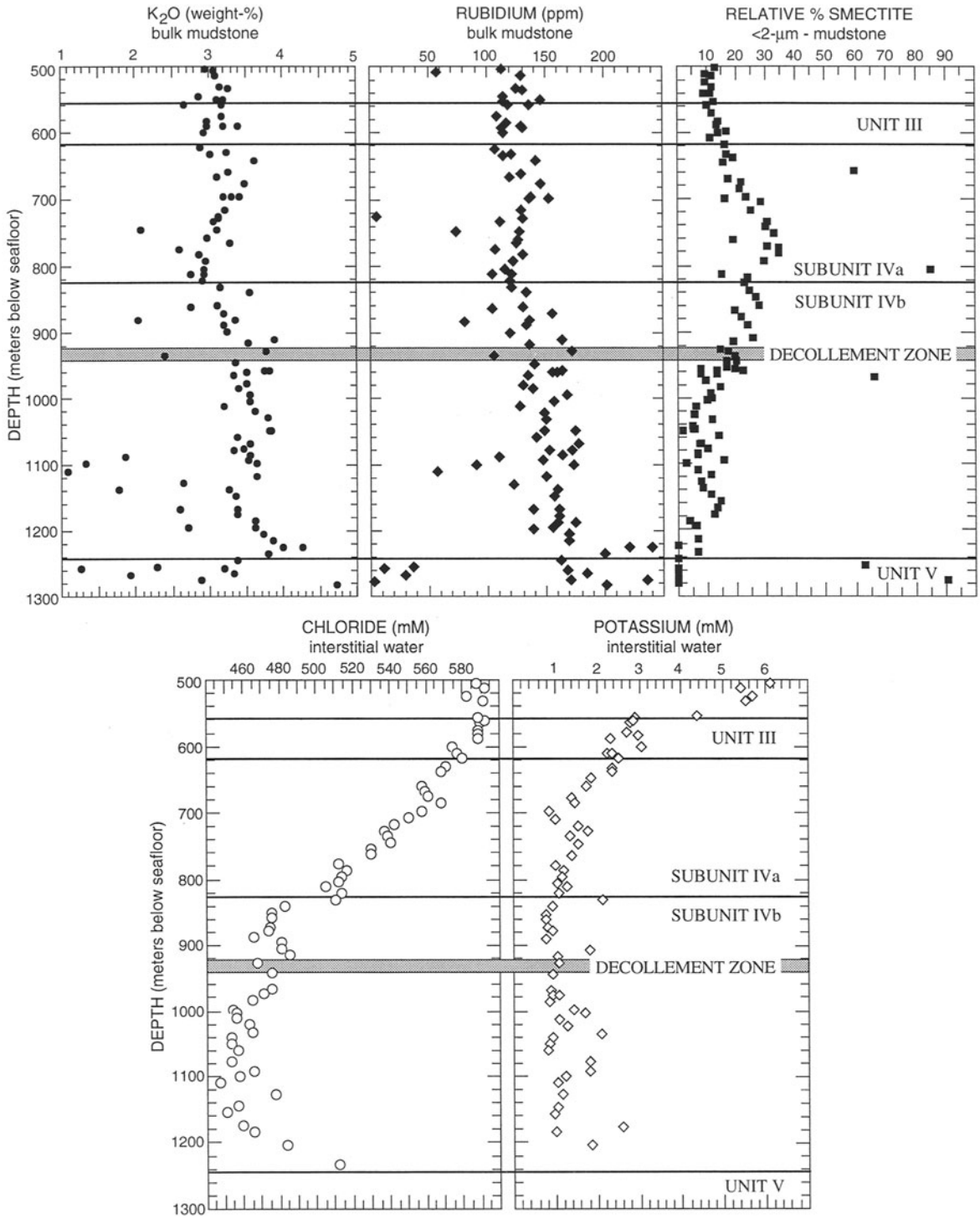

Figure 9. Comparisons of depth profiles for chloride and potassium (interstitial water), K_2O and Rb (bulk mudstones), and relative-% smectite (clay-sized fraction) at Site 808. Data are from Shipboard Scientific Party (1991), Pickering et al. (1993b) and Underwood et al. (1993a, 1993b).

https://doi.org/10.1346/CCMN.1996.0440304 Published online by Cambridge University Press

within the matrix of turbidites came from the same basic source as the clay minerals within hemipelagic muds.

Past investigations of sand provenance within the Nankai Trough and adjacent portions of Shikoku Basin have led most workers to conclude that the dominant sediment source area is located in the collision zone between the Izu-Bonin arc and the Honshu arc (Taira and Niitsuma 1986; Marsaglia et al. 1992). The Izu-Honshu collision zone provides a source for both neovolcanic and paleovolcanic rock fragments, recycled sedimentary and low-grade metasedimentary rock fragments, monocrystalline feldspar and abundant quartz. The Fuji River and Tenryu River drainage networks carry this detritus into the heads of the Suruga Trough and Tenryu Canyon (Figure 1). Our data show that the clay-sized sediments from the central segment of the Nankai Trough contain abundant detrital illite that was derived from source terranes exposed to conditions of anchimetamorphism, grading into lower greenschist-facies alteration. Based upon the low phengite content of the detrital micas, the P-T gradient within the source region must have been within the confines of the low-pressure facies series of metamorphism (Underwood et al. 1993a). Thus, mineralogic characteristics of the clay-sized detritus also match those of rocks types within the Izu-Honshu collision zone.

Shikoku Basin Clay Mineralogy

Collation of the estimated clay-mineral percentages at Site 808 with results from nearby DSDP sites are not strictly valid because of differences in analytical technique and peak-intensity weighting factors, although first-order trends can be compared. Cook et al. (1975) reported that illite is the most abundant clay mineral at both Site 297 (Shikoku Basin) and 298 (Nankai prism). Smectite (montmorillonite) values are subordinate, except within the Shikoku Basin at depths greater than 600 m, where relative percentages for the <2 μm size fraction increase from 45% to 57%. Chamley et al. (1986) likewise reported an illite-rich (30% to 50%) and chlorite-rich (20% to 35%) assemblage of clay minerals at Sites 582 and 583. Smectite increases to 25% to 40% within lower Pleistocene and Pliocene hemipelagic deposits of the Shikoku Basin (566 to 749 m). Smectite also increases considerably in Miocene mudstones cored from the lower parts of holes 442, 443 and 444 within the Shikoku Basin (Chamley 1980). Chamley (1980, 1986) reported occurrences of mixed-layer clays but did not calculate variations in I/S ratios.

Our most significant departure from the previous DSDP results is the reduction of discrete smectite beginning at a depth of about 800 mbsf (Figure 4). This stratigraphic position is deeper than the maximum penetration of previous DSDP holes, so we have no means of assessing whether or not the change is a regional phenomenon. Three reasonable explanations for the smectite depletion need to be considered: 1) a shift in detrital source areas during Pliocene time; 2) a change in the amount of volcanic activity and/or chemical weathering of volcanic rocks within the Pliocene source area(s); and 3) recent clay diagenesis within the Nankai accretionary prism, with alteration of discrete smectite to mixed-layer I/S. Of course, these explanations are not mutually exclusive.

Several observations lead us to conclude that subunit IVb contained less smectite, long before the effects of diagenesis were imparted. Smectite replacement of glass shards within discrete ash layers begins at a depth of ~200 mbsf. Below 550 mbsf the concentration of clay minerals (mostly smectite) within discrete ash layers increases dramatically (Masuda et al. 1993). Therefore, chemical conditions have been favorable to form authigenic smectite. However, discrete ash layers are scarce within subunit IVb. Presumably, the transition from subunit IVa to IVb also coincided with a down-section reduction in the amount of disseminated glass shards in the mudstones, thereby reducing the precursors for authigenic smectite. The upper boundary of subunit IVb marks an abrupt termination of zeolite mineralization within the bulk mudstones. This change is probably due to an absence or reduction of glass shards as a starting product for clinoptilolite. We believe that less detrital smectite was weathered and transported into the Shikoku Basin early in its history and less smectite was produced via *in situ* alteration of disseminated ash. However, it is also clear that illitization of both detrital and authigenic smectite components becomes increasingly significant with depth, such that specimens from below 900 mbsf typically contain more than 30% illite in the I/S phase. Consequently, clay diagenesis must also have contributed to the negative smectite gradient within subunit IVb, as discussed below.

Pyroclastic Contributions to Shikoku Basin

Some of the compositional variability displayed by mudrocks at Site 808 certainly could be due to inconsistent admixtures of disseminated volcanic ash, but the extent of this mixing can be evaluated geochemically. Chemical analyses of discrete ash deposits of Pliocene and Quaternary age yielded erratic but substantial departures from the bulk sediment geochemistry (Masuda et al. 1993). The range of observed Ti/Al-oxide ratios, for example, is approximately 0.010 to 0.050, and there is a pronounced decrease in this ratio within the ash-rich intervals of Unit III and subunit IVa (Figure 7). Overall, SiO_2 contents for ash range from 56% to 80% and silica/alumina ratios vary between about 2.5 and 7.5 (Masuda et al. 1993). The chemical heterogeneity of the pyroclastic material is consistent with the documented range of andesitic to

rhyolitic sources of explosive volcanism on the Japanese Islands. We agree with the assessment of Pouclet et al. (1986) who identified the active volcanic arc of southwest Japan, including the Izu-Honshu collision zone, as the principal source of Quaternary ash (Figure 1). Other possible sources would be the explosive volcanic centers on Kyushu and the Izu-Bonin arc.

H_4SiO_4 concentrations from interstitial waters decrease sharply between 550 and 600 mbsf (Shipboard Scientific Party 1991). Dissolution of volcanic glass from Unit III and subunit IVa may have removed this reactive component from the sediment with pore fluid advection leading to higher dissolved silica concentrations for overlying Unit II. As mentioned previously, partial alteration of glass shards to smectite is obvious within discrete ash layers (Shipboard Scientific Party 1991; Masuda et al. 1993). However, the chemical effects of the devitrification and illitization have not produced clear gradients for either bulk-ash or bulk-mudrock geochemistry (Figure 7). Moreover, because of the chemical homogeneity of mudstones throughout most of the Site 808 section (Figure 7), there is little chemical evidence to support the idea of mixing abundant pyroclastic debris into hemipelagites within either Unit III or subunit IVa.

In contrast to the heterogeneous ash deposits of Unit III and subunit IVa, all but one of the tuff beds within Unit V are highly siliceous. Most samples contain between 72% and 80% silica, and SiO_2/Al_2O_3 ratios are consistently greater than the average bulk mudstone from Site 808 (Figure 8). There is a marked chemical divergence between Unit V claystones and tuffs, which indicates that the multi-colored siliciclastic interbeds contain very little disseminated ash. These Miocene pyroclastic eruptions probably emanated from a single rhyolitic source, perhaps as part of the widespread phase of anomalous near-trench magmatism that affected the Outer Zone of southwest Japan between 15 Ma and 12 Ma (Oba 1977; Shibata and Ishihara 1979; Terakado et al. 1988; Hibbard and Karig 1990). Some of the Miocene eruptions evidently triggered subaqueous pyroclastic surges and high-concentration turbidity currents that moved well seaward of the paleo-subduction front.

Conditions Promoting Smectite-to-Illite Diagenesis

Peaks produced by disordered I/S (R = 0) first appear for data from mudstone samples at a stratigraphic position of ~555 mbsf (Figure 6). The estimated temperature at this depth bolsters our interpretation of diagenetic alteration of detrital and/or authigenic smectite to illite. The seafloor temperature at Site 808 is ~2 °C, and the average geothermal gradient recorded for the upper 350 m of the borehole is ~110 °C/km (Shipboard Scientific Party 1991). If we assume that this gradient remains linear to a depth of 560 mbsf, then the temperature associated with the beginning of illitization is ~65 °C. Similarly, the temperature extrapolated to 1200 mbsf would be ~130 °C. However, these temperatures are best viewed as maxima. If one assumes constant heat flow and considers the effects of increasing thermal conductivity with depth due to reduction of porosity, then the thermal gradient must be non-linear. Kastner et al. (1993) arrived at independent estimates of thermal conditions using the Mg-Li geothermometer. They calculated a temperature of 120 °C at a depth of 1200 mbsf, so an average gradient of approximately 110 °C/km appears to be reasonable.

Beginning at a depth of 900 mbsf (~100 °C), the I/S phase at Site 808 typically contains greater than 30% illite (Figure 6). The initial appearance of R = 1 ordering in the <2 μm size fraction occurs at a depth of approximately 1220 m (~135 °C). In most sedimentary basins, the transition from random to ordered interlayers occurs with 60 to 70% illite layers (Bethke et al. 1986), and the results from Site 808 are consistent with this norm (Figure 6). Within the finer size fraction (<0.2 μm), R = 1 ordering first appears at a shallower depth of about 1060 mbsf and at an estimated temperature of 120 °C. This acceleration of illitization within the finer size fraction is also typical (Hower et al. 1976; Jennings and Thompson 1986).

Temperature appears to be the most important variable for the smectite-to-illite transition. The reaction is affected by many other internal and external factors, such as hydraulic and differential burial pressures, host-rock porosity and permeability, water-rock ratios, pore water chemistry, abundance of specific interlayer cations in the smectite, bulk host-rock mineralogy, the nature of lithologic interbedding, chemical composition of the precursor smectite, content of organic matter and reaction time (Hower et al. 1976; Eberl and Hower 1976; Eberl 1978; Roberson and Lahann 1981; Bruce 1984; Colten-Bradley 1987; Yau et al. 1987; Velde and Iijima 1988; Velde and Espitalie 1989; Whitney 1990). Empirical correlations of I/S ratios with burial temperature and heating time indicate that reaction progress can be modeled according to kinetic rate laws (Eberl and Hower 1976; Bethke and Altaner 1986; Pytte and Reynolds 1989; Huang et al. 1993). Because so many variables are involved, it is not surprising that starting temperatures and gradients of illitization both vary from one borehole site to another (Perry and Hower 1970; Dypvik 1983; Bruce 1984; Ramseyer and Boles 1986; Velde and Iijima 1988; Freed and Peacor 1989a). On the Gulf Coast of the United States, for example, the temperature range for onset of illitization extends from 58 to 92 °C, and I/S ratios reach from 70 to 80% illite at temperatures of 88 to 142 °C (Freed and Peacor 1989a). Tribble (1990) documented an intriguing example from the Barbados accretionary prism, in which illitization apparently begins at temperatures as low as 24 °C (Schoonmaker et al. 1986). Data from the Nankai accretionary prism are

well within the anticipated window of burial temperature (60 to 90 °C). Consequently, we see no reason to invoke special hydrogeochemical circumstances to account for the diagenetic trend at Site 808.

According to kinetic models, I/S reaction rates slow down considerably as the mixed-layer composition approaches that of pure illite (Bethke and Altaner 1986; Pytte and Reynolds 1989; Huang et al. 1993). Higher activation energies are associated with highly illitic I/S, which provides one explanation for why mixed-layer phases with 15 to 20% expandable layers persist well beyond the so-called completion temperature. Many of the empirical I/S gradients and modeled curves of smectite-to-illite conversion show pronounced S-shapes (Huang et al. 1993). The I/S data from Site 808 define a fairly linear trend that ends at 75 to 80% illite (Figure 6). A second factor to consider is the potential depletion of K-bearing minerals in host mudrocks or in adjacent deposits. Dissolution of K-feldspar, for example, commonly provides for the required uptake of potassium and aluminum by illite crystallites (Perry and Hower 1970; Hower et al. 1976; Bruce 1984; Jennings and Thompson 1986). At Site 808, dissolved potassium is reduced to concentrations of less than 2 mM/L, but the supply below 600 mbsf is by no means exhausted (Figure 9). Consequently, we conclude that burial within and beneath the Nankai prism toe has not been deep enough to reach the illitization completion temperature.

The type of I/S ordering is also sensitive to several variables including the geothermal gradient. The change from R = 0 (disordered) to R = 1 (ordered) I/S, for example, can occur at burial temperatures as low as 50 to 80 °C, particularly where geothermal gradients are relatively low (Velde et al. 1986). In other first-cycle basins, random (R = 0) ordering persists to temperatures of 100 to 130 °C even with geothermal gradients of 25 to 30 °C/km (Velde and Iijima 1988; Hansen and Lindgreen 1989). Data from active continental geothermal fields seem to provide the best match for the results at Site 808. The geothermal sites prove that I/S reactions can move to completion within sediments that are only 1 to 2 Ma in age, but the temperatures required for R = 1 ordering under these circumstances are between 135 and 155 °C (Jennings and Thompson 1986; Walker and Thompson 1990). Peak temperatures for the Shikoku Basin hemipelagic facies were attained only within the last 0.4 m.y. after rapid accumulation of the overlying turbidite wedge and thrust imbrication. Thus, ordering of I/S clays at Site 808 probably has been retarded somewhat by insufficient heating times.

Influence of Illitization on Nankai Hydrogeochemistry

Two of the more important aspects of the smectite-to-illite transformation involve the release of interlayer water into the pore system of the host mudrock and the development of excess pore-fluid pressures if low mudrock permeabilities inhibit dissipation of the liberated water (Burst 1969; Bruce 1984; Colten-Bradley 1987; Freed and Peacor 1989b; Vrolijk 1990). In the case of the Nankai accretionary prism, we know that the depth interval containing I/S clays coincides with a decrease in interstitial water chlorinity (Shipboard Scientific Party 1991; Kastner et al. 1993). Chloride content begins to decrease gradually from maxima of approximately 590 mM at 560–580 mbsf to minima of 450 mM at 1040–1080 mbsf, and there is a deflection in the gradient at about 820 mbsf (Figure 9). Sodium content displays the same trend. One important question to answer is whether or not the freshening of pore water can be attributed to *in situ* dehydration of smectite. A more difficult question is whether or not the change in the chlorinity gradient at about 820 mbsf is related to a decrease in the rate at which smectite alters to I/S.

Vrolijk et al. (1991) summarized a method for mass balance calculations of chloride dilution in response to clay mineral diagenesis. Three variables need to be considered: 1) bulk porosity; 2) percentage of smectite in the total solid fraction; and 3) percentage of the interlayer water expelled from the smectite. Except for the local occurrences of bentonitic layers within Unit IV, the relative percentages of smectite within the clay-mineral population at Site 808 are no higher than about 35% for the <2 μm size fraction and 25% for the 2 to 6 μm size fraction. When data from shipboard XRD analyses of bulk powders (Shipboard Scientific Party 1991) are combined with the clay mineralogy reported herein, it seems clear that smectite averages less than 10% of the bulk mudstone. If allowances are made for amorphous constituents undetected by XRD, such as opaline silica and volcanic glass, then the volume of expandable clay within the starting material becomes even lower, probably less than 5% of the average bulk mudstone.

Porosity values at Site 808, over the depth interval of 560–1080 mbsf, range from 45% down to 30% (Shipboard Scientific Party 1991). If one assumes a porosity value of 30%, together with 50% expulsion of interlayer water via transformation to a mixed-layer I/S, then roughly 50% of the original bulk-solid volume must be composed of smectite to dilute the chlorinity by 23% (590 mM to 450 mM). Increasing the water-expulsion value to 100% (complete transformation to illite with loss of both interlayer water and structural water) still requires a bulk-mud smectite concentration of 25%. Smectite concentrations appear to be too low to accomplish this, and the progression of illitization reactions at Site 808 are not advanced enough to account for the dilution of pore-water chlorinity via *in situ* dehydration of clay minerals. Moreover, alteration of volcanic ash to authigenic smectite

and zeolites, particularly within subunit IVa, should have consumed substantial amounts of H_2O, perhaps equivalent to >3% seawater concentration (Kastner et al. 1993). Assessing the possible influence of reaction rate seems unnecessary given the obvious mass-balance deficiency of smectite. We conclude that the low-chlorinity pore water extracted from Site 808 was imported from other portions of the Nankai accretionary prism.

Rather than forming in place, it is logical to suggest that diluted pore fluids migrated from deeper in the prism, where porosities are lower than 30%. One possible migration pathway is the décollement zone, within which permeabilities are enhanced by a penetrative scaly fabric of closely spaced fractures (Moore 1989; Moore and Vrolijk 1992). Direct evidence for active fluid advection along the décollement is lacking, but Kastner et al. (1993) demonstrated how an intense transient pulse could have injected low-salinity fluid roughly 300,000 years ago followed by diffusive downward migration. However, the décollement pathway is not necessarily mandated by the data. Slow movement may have been centered near the depth of the chloride concentration minimum, or there could have been mixing between two advective systems, one focused at the chloride minimum, the other at the 820 mbsf lithologic boundary between subunits IVa and IVb. This final hypothesis is supported by changes in ^{18}O, D and Sr isotopes across the décollement zone (Kastner et al. 1993). Fluids below the décollement probably were derived from deep-seated portions of the subduction zone, where underplated mixtures of lower Shikoku Basin mudstones and rhyolitic tuffs have been subjected to more advanced stages of illitization.

Only one site was drilled during Leg 131. We have no means of documenting the possible effects of strike-parallel fluid migration. The documented gradients from borehole temperature and near-surface heat flow certainly are high enough all along the strike of the subduction front to promote widespread smectite dehydration, beginning within the 600 to 1200 mbsf depth interval (Yamano et al. 1984, 1992; Ashi and Taira 1993). However, heat flow decreases with distance toward the shoreline of southwest Japan, which depresses the ideal temperature window for illitization deeper. Without knowing the exact subduction/accretion trajectories for given parcels of mudstone, it is almost impossible to predict when or where the ideal temperature conditions for clay-mineral dehydration will be encountered or how fluid pressure gradients might vary in response. The residence time within the ideal temperature window also must be balanced against the effects of all kinetic parameters. A unique solution to this problem seems unattainable given the existing data. As an additional complication, clay-mineral data from DSDP sites within the Shikoku Basin (Chamley 1980) indicate that many intervals of the abyssal-floor stratigraphy are more enriched with smectite than the hemipelagic muds at Site 808. Therefore, the possibility of a lateral component of fluid flux, from a smectite-rich compartment near the prism toe, also should be considered in assessments of the fluid budget.

SUMMARY AND CONCLUSIONS

Illite is the most abundant clay mineral in the Nankai accretionary prism. Relative percentages of the major mineral constituents (illite, chlorite and smectite) are remarkably uniform throughout the turbidite wedge, and there are no meaningful differences between clays in hemipelagic muds and turbidites. A modest amount of mineral partitioning occurs as a function of grain size with chlorite increasing for the 2 to 6 μm fraction and smectite increasing for the <2 μm fraction.

The Izu-Honshu collision zone served as the principal detrital source region for the trench-wedge deposits at Site 808. Most of the polymictic sediments (all size fractions) probably were eroded from within the Fuji River drainage basin and funneled through the Suruga Trough before entering the trench environment. A substantial fraction could also be derived from the Tenryu River and submarine canyon system, which is located immediately to the west of the collision zone.

The same basic detrital assemblage is characteristic of the underlying hemipelagic deposits of the Shikoku Basin. Unlike some other subduction zones, there are no deviations in clay mineralogy within the décollement zone. Smectite content increases monotonically within the upper Shikoku Basin facies (subunit IVa). This enrichment can be attributed, in part, to diagenetic alteration of disseminated volcanic ash. Smectite decreases relative to other clay minerals beginning at a depth of about 800 mbsf because there were lesser amounts of detrital smectite and volcanic ash transported into Shikoku Basin early in its history (subunit IVb). Also, burial temperatures within the past 0.4 m.y. reached levels high enough to initiate the transformation of smectite to illite at depths below 550 to 600 mbsf.

Most of the hemipelagic mudstones at Site 808 display uniform chemical compositions. Slight increases in K_2O and Rb within the Shikoku Basin facies are probably due to uptake of those cations by illite layers in I/S clays. For the most part, dissemination of volcanic ash into the background mud did not result in significant departures from the average bulk mudstone geochemistry. Geochemical divergence among interbeds is particularly pronounced between rhyolitic tuffs and variegated claystones of Unit V, which formed during juvenile stages of sedimentation above the basaltic basement. Tuff beds from Unit V correlate chemically and temporally with anomalous near-trench

magmatic bodies throughout the Outer Zone of southwest Japan.

The illite content of I/S mixed-layer clay increases steadily down-section within the Shikoku Basin facies. The initial appearance of random (R = 0) I/S occurs at a depth of approximately 555 m where the present-day temperature is ~65 °C. R = 1 ordering for the <2 μm size fraction first occurs at a depth of 1220 mbsf and a temperature of ~135 °C. Within the <0.2 μm size fraction, R = 1 ordering first appears at a depth of 1060 mbsf and a temperature of ~120 °C. This illitization gradient is most consistent with data from sedimentary basins where geothermal gradients are abnormally high, which define active geothermal fields. However, burial depths beneath the toe of the accretionary prism have not been sufficient to reach the so-called completion temperature of illitization.

The increase of illite interlayers in I/S mixed-layer clays occurs over the same depth interval as a 23% reduction in pore-water chlorinity. The absolute abundance of smectite in the Shikoku Basin section (Unit IV) appears to be much too small to generate the necessary dilution through *in situ* smectite dehydration. Therefore, low-chlorinity pore waters probably migrated from deeper and more landward zones of underplating where lower porosities and/or higher smectite percentages are likely. Alternatively, some strike-parallel fluid migration may have occurred near the prism toe from pockets of Shikoku Basin mudstone containing greater percentages of detrital and authigenic smectite.

ACKNOWLEDGMENTS

We thank the crew and staff aboard the D/V JOIDES Resolution for their assistance during sample acquisition. XRF analyses were completed by N. Marsh and B. Dickie and funded by the Department of Geology at the University of Leicester. The XRD analyses were completed by R. Orr at the University of Missouri, with funding provided by the National Science Foundation through the Joint Oceanographic Institutions, U.S. Science Support Program. E. Hathon and D. Bergfeld assisted in the lab. K. Marsaglia, S. O'Connell, P. Vrolijk, R. C. Reynolds and D. R. Pevear provided useful comments.

REFERENCES

Ashi J, Taira A. 1993. Thermal structure of the Nankai accretionary prism as inferred from the distribution of gas hydrate BSRs. In: Underwood MB, editor, Thermal evolution of the Tertiary Shimanto Belt, Southwest Japan: An example of ridge-trench interaction. Geol Soc Am Spec Paper 273:137–149.

Bethke CM, Altaner SP. 1986. Layer-by-layer mechanism of smectite illitization and application to a new rate law. Clays & Clay Miner 34:136–145.

Bethke CM, Vergo N, Altaner SP. 1986. Pathways of smectite illitization. Clays & Clay Miner 34:125–135.

Biscaye PE. 1965. Mineralogy and sedimentation of recent deep-sea clay in the Atlantic Ocean and adjacent seas and oceans. Geol Soc Am Bull 76:803–831.

Blake, MC, Jr., Jayko AS, McLaughlin RJ. 1985. Tectonostratigraphic terranes of the northern Coast Ranges, California. In: Howell DG, editor. Tectonostratigraphic terranes of the Circum-Pacific Region, Circum-Pacific Council for Energy & Min. Res. Earth Sci Series 1:159–172.

Boggs, S, Jr. 1984. Quaternary sedimentation in the Japan arc-trench system. Geol Soc Am Bull 95:669–685.

Bruce CH. 1984. Smectite dehydration—its relation to structural development and hydrocarbon accumulation in northern Gulf of Mexico basin. Am Assoc Pet Geol Bull 68: 673–683.

Burst JF. 1969. Diagenesis of Gulf Coast clayey sediments and its possible relation to petroleum migration. Am Assoc Pet Geol Bull 53:73–93.

Cadet J-P, Kobayashi K, Aubouin J, Boulegue J, Deplus C, Dulsais J, von Huene R, Jolivet L, Kanazawa T, Kasahara J, Koizumi K, Lallemand S, Nakamura Y, Pautot G, SuyehiroK, Tani S, Tokuyama H, Yamazaki T. 1987. The Japan Trench and its juncture with the Kuril Trench: Cruise results of the Kaiko project, Leg 3. Earth & Planet Sci Lett 83:267–284.

Chamley H. 1980. Clay sedimentation and paleoenvironment in the Shikoku Basin since the middle Miocene (Deep Sea Drilling Project Leg 58, North Philippine Sea). In: Klein Gde V, Kobayashi JW, editors. Init. Repts. DSDP Washington, D.C.: U.S. Govt. Printing Office. 58:669–681.

Chamley H, Cadet J-P, Charvet J. 1986. Nankai Trough and Japan Trench late Cenozoic paleoenvironments deduced from clay mineralogy data. In: Kagami H, Karig DE, Coulbourn WT, editors. Init. Repts. DSDP Washington, D.C.: U.S. Govt. Printing Office. 87:633–642.

Chamot-Rooke N, Renard V, Le Pichon X. 1987. Magnetic anomalies in the Shikoku Basin: A new interpretation. Earth & Planet Sci Lett 83:214–228.

Colten-Bradley VA. 1987. Role of pressure in smectite dehydration—effects on geopressure and smectite-to-illite transformation. Am Assoc Pet Geol Bull 71:1414–1427.

Cook HE, Zemmels I, Matti JC. 1975. X-ray mineralogy data, far western Pacific, Leg 31 Deep Sea Drilling Project. In: Karig DE, Ingle, Jr. JC, et al., editors. Init. Repts. DSDP Washington, D.C.: U.S. Govt. Printing Office. 31:883–895.

Coulbourn WT. 1986. Sedimentologic summary, Nankai Trough Sites 582 and 583, and Japan Trench Site 584. In: Kagami H, Karig DE, Coulbourn WT, editors. Init. Repts. DSDP Washington, D.C.: U.S. Govt. Printing Office, 87: 909–926.

De Rosa R, Zuffa GG, Taira A, Leggett JK. 1986. Petrography of trench sands from the Nankai Trough, southwest Japan: Implications for long-distance turbidite transportation. Geol Mag 123:477–486.

Donnelly TW. 1980. Chemical composition of deep sea sediments—Sites 9 through 425, Legs 2 through 54. In: Rosendahl BR, Hekinian R, et al., editors. Init. Repts. DSDP Washington, D.C.:U.S. Govt. Printing Office. 54:899–949.

Dypvik H. 1983. Clay mineral transformations in Tertiary and Mesozoic sediments from North Sea. Am Assoc Pet Geol Bull 67:160–165.

Eberl DD. 1978. The reaction of montmorillonite to mixed-layer clay: The effect of interlayer alkali and alkaline earth cations. Geochim Cosmochim Acta 42:1–7.

Eberl D, Hower J. 1976. Kinetics of illite formation. Geol Soc Am Bull 87:1326–1330.

Freed RL, Peacor DR. 1989a. Variability in temperature of the smectite/illite reaction in Gulf Coast sediments. Clay Miner 24:171–180.

Freed RL, Peacor DR. 1989b. Geopressured shale and sealing effect of smectite to illite transition. Am Assoc Pet Geol Bull 73:1223–1232.

Gieskes JM, Gamo T, Kastner M. 1993. Major and minor element geochemistry of interstitial waters of Site 808, Nankai Trough: An overview. In: Hill IA, Taira A, Firth

JV, et al. editors. Proc. ODP, Sci. Results Ocean Drilling Program, College Station. 131:387–396.
Gorsline DS. 1984. A review of fine-grained sediment origins, characteristics, transport and deposition. In: Stow DAV, Piper DJW, editors. Fine-grained sediments: Deep water processes and facies. Oxford: Blackwell Sci Publ. p 17–34.
Gorsline DS. 1985. Some thoughts on fine-grained sediment transport and deposition. Sed Geol 41:113–130.
Hansen PL, Lindgreen H. 1989. Mixed-layer illite/smectite diagenesis in Upper Jurassic claystones from the North Sea and onshore Denmark. Clay Miner 24:197–213.
Hathon EG. 1992. X-ray diffraction and transmission electron microscopy study of the surface charge on the illite and smectite components of illite/smectite mixed-layer clays. [unpublished Ph.D. Dissertation]. Columbia: University of Missouri. 215 p.
Hathon EG, Underwood MB. 1991. Clay mineralogy and chemistry as indicators of hemipelagic sediment dispersal south of the Aleutian arc. Marine Geol 97:145–166.
Hibbard JP, Karig DE. 1990. Alternative plate model for the Early Miocene evolution of the SW Japan margin. Geology 18:170–174.
Hower J, Eslinger EV, Hower ME, Perry EA. 1976. Mechanism of burial metamorphism of argillaceous sediment: 1. mineralogical and chemical evidence. Geol Soc Am Bull 87:725–737.
Huang W-L, Longo JM, Pevear DR. 1993. An experimentally derived kinetic model for smectite-to-illite conversion and its use as a geothermometer. Clays & Clay Miner 41: 162–177.
Inoue A, Bouchet A, Velde B, Meunier A. 1989. Convenient technique for estimating smectite layer percentage in randomly interstratified illite/smectite minerals. Clays & Clay Miner 37:227–234.
Jennings S, Thompson GR. 1986. Diagenesis of Plio-Pleistocene sediments of the Colorado River Delta, southern California. J Sed Pet 56:89–98.
Kagami H, Karig DE, Coulbourn WT, Bray CJ, Charvet J. 1986. Init. Repts. DSDP Washington, D.C.: U.S. Govt. Printing Office. 87:985.
Karig DE, Ingle, Jr. JC, Haile N, Bouma AH, Moore JC, White SM, MacGregor I, Ellis H, Ujiie H, Ling HY, Koizumi I, Watanabe T, Yasui M. 1975. In: Karig DE, Ingle Jr, JC, editors. Init. Repts. DSDP Washington, D.C.: U.S. Govt. Printing Office. 31:927.
Kastner M, Elderfield H, Jenkins WJ, Gieskes JM, Gamo T. 1993. Geochemical and isotopic evidence for fluid flow in the western Nankai subduction zone, Japan. In: Hill IA, Taira A, Firth JV, et al., editors. Proc. ODP, Sci. Results. Ocean Drilling Program, College Station. 131:397–416.
Kawahata H, Fujioka K, Ishizuka T. 1986. Sediments and interstitial water at Sites 582 and 584, the Nankai Trough and the Japan Trench landward slope. In: Kagami H, Karig DE, Coulbourn WT, et al., editors. Init. Repts. DSDP. Washington, D.C.:U.S. Govt. Printing Office. 87:865–875.
Klein G deV, Kobayashi JW, Chamley H, Curtis D, Dick H, Echols DJ, Fountain DM, Kinoshite H, March NG, Mizuno A, Nisterenko GV, Okada H, Sloan JR, Waples D, White SM. 1980. Init. Repts. DSDP Washington, D.C.: U.S. Govt. Printing Office. 58:1022 p.
Le Pichon X, Iiyama T, Chamley H, Charvet J, Faure M, Fujimoto H, Furuta T, Ida Y, Kagami H, Lallemant S, Leggett J, Murata A, Okada H, Rangin C, Renard V, Taira A, Tokuyama H. 1987a. Nankai Trough and the fossil Shikoku Ridge: Results of Box 6 Kaiko survey. Earth & Planet Sci Lett 83:186–198.
Le Pichon X, Iiyama T, Chamley H, Charvet J, Faure M, Fujimoto H, Furuta T, Ida Y, Kagami H, Lallemant S, Leggett J, Murata A, Okada H, Rangin C, Renard V, Taira A, Tokuyama H. 1987b. The eastern and western ends of Nankai Trough: Results of Box 5 and Box 7 Kaiko survey. Earth & Planet Sci Lett 83:199–213.
Marsaglia KM, Ingersoll RV, Packer BM. 1992. Tectonic evolution of the Japanese Islands as reflected in modal compositions of Cenozoic forearc and backarc sand and sandstone. Tectonics 11:1028–1044.
Masuda H, Tanaka H, Gamo T, Soh W, Taira A. 1993. Major-element chemistry and alteration mineralogy of volcanic ash. Site 808 in the Nankai Trough. In: Hill IA, Taira A, Firth JV, et al., editors. Proc. ODP, Sci. Results Ocean Drilling Program, College Station. 131:175–184.
McManus DA. 1991. Suggestions for authors whose manuscripts include quantitative clay mineral analysis by X-ray diffraction. Mar Geol 98:1–5.
Minai Y, Matsumoto R, Tominaga T. 1986. Geochemistry of deep sea sediments from the Nankai Trough, the Japan Trench, and adjacent regions. In: Kagami H, Karig DE, Coulbourn WT, et al., editors. Init. Repts. DSDP. Washington, D.C.:U.S. Govt. Printing Office. 87:643–657.
Moore DM, Reynolds, RC, Jr. 1989. X-ray diffraction and the identification and analysis of clay minerals. New York: Oxford University Press. 332 p.
Moore GF, Shipley TH, Stoffa PL, Karig DE, Taira A, Kuramoto S, Tokuyama H, Suyehiro K. 1990. Structure of the Nankai Trough accretionary zone from multichannel seismic reflection data. J Geophys Res 95:8753–8765.
Moore JC. 1989. Tectonics and hydrogeology of accretionary prisms: Role of the décollement zone. J Struc Geol 11: 95–106.
Moore JC, Karig DE. 1976. Sedimentology, structural geology, and tectonics of the Shikoku subduction zone, southwestern Japan. Geol Soc Am Bull 87:1259–1268.
Moore JC, Byrne T, Plumley PW, Reid M, Gibbons H, Coe RS. 1983. Paleogene evolution of the Kodiak Islands, Alaska: Consequences of ridge-trench interaction in a more southerly latitude. Tectonics 2:265–293.
Moore JC, Mascle A, Taylor E, Andreieff P, Alvarez F, Barnes R, Beck C, Behrmann J, Blanc G, Brown K, Clark M, Dolan J, Fisher A, Gieskes J, Hounslow M, McLellan P, Moran K, Ogawa Y, Sakai T, Schoonmaker J, Vrolijk P, Wilkens R, Williams G. 1988. Tectonics and hydrogeology of the northern Barbados Ridge: Results from Ocean Drilling Program Leg 110. Geol Soc Am Bull 100:1578–1593.
Moore JC, Vrolijk P. 1992. Fluids in accretionary prisms. Rev Geophys 30:113–135.
Nakamura K, Renard V, Angelier J, Azema J, Bourgois J, Deplus C, Fujioka K, Hamano Y, Huchon P, Kinoshita H, Labaume P, Ogawa Y, Seno T, Takeuchi A, Tanahashi M, Uchiyama A, Vigneresse J-L. 1987. Oblique and near collision subduction, Sagami and Suruga Troughs—preliminary results of the French-Japanese 1984 Kaiko cruise, Leg 2. Earth & Planet Sci Lett 83:229–242.
Oba N. 1977. Emplacement of granitic rocks in the Outer Zone of southwest Japan and geological significance. J Geol 85:383–393.
Ogawa Y, Horiuchi K, Taniguchi H, Naka J. 1985. Collision of the Izu arc with Honshu and the effects of oblique subduction in the Miura-Boso Peninsulas. Tectonophysics 119: 349–379.
Ogawa Y, Taniguchi H. 1988. Geology and tectonics of the Miura-Boso Peninsulas and the adjacent area. Modern Geol 12:147–168.
Okuda Y, Honza E. 1988. Tectonic evolution of the Seinan (SW) Japan fore-arc and accretion in the Nankai Trough. Modern Geol 12:411–434.
Perry E, Hower J. 1970. Burial diagenesis in Gulf Coast pelitic sediments. Clays & Clay Miner 18:165–177.

Pickering KT, Underwood MB, Taira A. 1992. Open-ocean to trench turbidity-current flow in the Nankai Trough: Flow collapse and reflection. Geology 20:1099–1102.

Pickering KT, Underwood MB, Taira A. 1993a. Stratigraphic synthesis of the DSDP-ODP sites in the Shikoku Basin, Nankai Trough, and accretionary prism. In: Hill IA, Taira A, Firth JV, et al., editors. Proc. ODP, Sci. Results Ocean Drilling Program, College Station. 131:313–330.

Pickering KT, Marsh NG, Dickie B. 1993b. Data Report: Inorganic major, trace, and rare earth element analyses of the muds and mudstones from Site 808. In: Hill IA, Taira A, Firth JV, et al., editors. Proc. ODP, Sci. Results Ocean Drilling Program, College Station. 131:427–450.

Piper DJW, von Huene R, Duncan JR. 1973. Late Quaternary sedimentation in the active eastern Aleutian Trench. Geology 1:19–22.

Pouclet A, Fujioka K, Charvet J, Cadet J-P. 1986. Petrography and geochemistry of volcanic ash layers from Leg 87A, Nankai Trough (south Japan). In: Kagami H, Karig DE, Coulbourn WT, et al., editors. Init. Repts. DSDP. Washington, D.C.: U.S. Govt. Printing Office. 87:695–701.

Pytte AM, Reynolds RC. 1989. The thermal transformation of smectite to illite. In: Naeser ND, McCulloh TH, editors. Thermal history of sedimentary basins. New York: Springer-Verlag. p 133–140.

Ramseyer K, Boles JR. 1986. Mixed-layer illite/smectite minerals in Tertiary sandstones and shales, San Joaquin Basin, California. Clays & Clay Miner 34:115–124.

Reynolds, RC, Jr., Hower J. 1970. The nature of interlayering in mixed-layer illite-montmorillonites. Clays & Clay Miner 18:25–36.

Roberson HE, Lahann RW. 1981. Smectite to illite conversion rates: Effects of solution chemistry. Clays & Clay Miner 29:129–135.

Schweller WJ, Kulm LD. 1978. Depositional patterns and channelized sedimentation in active eastern Pacific trenches. In: Stanley DJ, Kelling G, editors. Sedimentation in submarine canyons, fans, and trenches. Stroudsburg:Dowden, Hutchinson, and Ross. p 323–350.

Schoonmaker J, Mackenzie FT, Speed RC. 1986. Tectonic implications of illite/smectite diagenesis, Barbados accretionary prism. Clays & Clay Miner 34:465–472.

Shibata K, Ishihara S. 1979. Initial $^{87}Sr/^{86}Sr$ ratios of plutonic rocks from Japan. Contrib Mineral Petrol 70:381–390.

Shimamura K. 1989. Topography and sedimentary facies of the Nankai deep sea channel. In: Taira A, Masuda F, editors. Sedimentary facies in the active plate margin. Tokyo: Terra Sci Publ Co. p 529–556.

Shipboard Scientific Party. 1991. Site 808. In: Taira A, Hill I, Firth J, et al. editors. Proc. ODP, Initial Results Ocean Drilling Program, College Station. 131:71–269.

Soh W, Pickering KT, Taira A, Tokuyama H. 1991. Basin evolution in the arc-arc Izu Collision Zone, Mio-Pliocene, Miura Group, central Japan. J Geol Soc London 148:317–330.

Srodon J. 1980. Precise identification of illite/smectite interstratifications by X-ray powder diffraction. Clays & Clay Miner 28:401–411.

Srodon J. 1981. X-ray identification of randomly interstratified illite-smectite in mixtures with discrete illite. Clay Miner 16:297–304.

Starkey HC, Blackmon PD, Hauff PC. 1984. The routine mineralogical analysis of clay bearing samples. U.S. Geol Surv Bull 1563:1–32.

Taira A, Niitsuma N. 1986. Turbidite sedimentation in the Nankai Trough as interpreted from magnetic fabric, grain size, and detrital modal analyses. In: Kagami H, Karig DE, Coulbourn WT, et al., editors. Init. Repts. DSDP. Washington, D.C.: U.S. Govt. Printing Office. 87:611–632.

Taira A, Hill I, Firth J, Berner U, Bruckmann W, Byrne T, Chabernaud T, Fisher A, Foucher J-P, Gamo T, Gieskes J, Hyndman R, Karig D, Kastner M, Kato Y, Lallemant S, Lu R, Maltman A, Moore G, Moran K, Olaffson G, Owens W, Pickering K, Siena F, Taylor E, Underwood M, Wilkinson C, Yamano M, Zhang J. 1992. Proc. ODP, Initial Reports Ocean Drilling Program, College Station. 131:434 p.

Taira A, et al. 1992. Sediment deformation and hydrogeology of the Nankai Trough accretionary prism: Synthesis of shipboard results of ODP Leg 131. Earth & Planet Sci Lett 109:431–450.

Taira A, Katto J, Tashiro M, Okamura M, Kodama K. 1988. The Shimanto Belt in Shikoku, Japan: Evolution of cretaceous to Miocene accretionary prism. Mod Geol 12:5–46.

Terakado Y, Shimizu H, Masuda A. 1988. Nd and Sr isotopic variations in acidic rocks formed under a pecular tectonic environment in Miocene SW Japan. Contrib Mineral Petrol 99:1–10.

Toriumi M, Arai T. 1989. Metamorphism of the Izu-Tanzawa collision zone. Tectonophysics 160:293–303.

Tribble JS. 1990. Clay diagenesis in the Barbados accretionary complex: Potential impact on hydrology and subduction dynamics. In: Moore JC, Mascle A, Taylor E, Underwood MB, editors. Proc. ODP, Sci. Results Ocean Drilling Program, College Station. 110:97–110.

Underwood MB. 1986. Transverse infilling of the central Aleutian Trench by unconfined turbidity currents. Geo-Mar Lett 6:7–13.

Underwood MB. 1991. Submarine canyons, unconfined turbidity currents, and sedimentary bypassing of forearc regions. Rev Aquatic Sci 4:149–200.

Underwood MB, Norville C. 1986. Deposition of sand in a trench-slope basin by unconfined turbidity currents. Mar Geol 71:383–392.

Underwood MB, Orr R, Pickering K, Taira A. 1993a. Provenance and dispersal patterns of sediments in the turbidite wedge of Nankai Trough. In: Hill IA, Taira A, Firth JV, et al., editors. Proc. ODP, Sci. Results Ocean Drilling Program, College Station. 131:15–34.

Underwood MB, Pickering K, Gieskes JM, Kastner M, Orr R. 1993b. Sediment geochemistry, clay mineralogy, and diagenesis: A synthesis of data from Leg 131, Nankai Trough. In: Hill IA, Taira A, Firth JV, et al., editors. Proc. ODP, Sci. Results Ocean Drilling Program, College Station. 131:343–363.

Velde B, Iijima A. 1988. Comparison of clay and zeolite mineral occurrences in Neogene age sediments from several deep wells. Clays & Clay Miner 36:337–342.

Velde B, Espitalie J. 1989. Comparison of kerogen maturation and illite/smectite composition in diagenesis. J Petrol Geol 12:103–110.

Velde B, Suzuki T, Nicot E. 1986. Pressure-temperature-composition of illite/smectite mixed-layer minerals: Niger Delta mudstones and other examples. Clays & Clay Miner 34:435–441.

von Huene R, Arthur MA. 1982. Sedimentation across the Japan Trench off northern Honshu Island. In: Leggett JK, editor. Trench-forearc geology. Geol Soc London Spec Publ 10:27–48.

Vrolijk P. 1990. On the mechanical role of smectite in subduction zones. Geology 18:703–707.

Vrolijk P, Fisher A, Gieskes J. 1991. Geochemical and geothermal evidence for fluid migration in the Barbados accretionary prism (ODP Leg 110). Geophys Res Lett 18: 947–950.

Walker JR, Thompson GR. 1990. Structural variations in chlorite and illite in a diagenetic sequence from the Imperial Valley, California. Clays & Clay Miner 38:315–321.

Whitney G. 1990. Role of water in the smectite-to-illite reaction. Clays & Clay Miner 38:343–350.
Yamano M, Uyeda S, Aoki Y, Shipley TH. 1982. Estimates of heat flow derived from gas hydrates. Geology 10:339–343.
Yamano M, Honda S, Uyeda S. 1984. Nankai Trough: A hot trench? Mar Geophys Res 6:187–203.
Yamano M, Foucher J-P, Kinoshita M, Fisher A, Hyndman RD. ODP Leg 131 Shipboard Scientific Party. 1992. Heat flow and fluid flow regime in the western Nankai accretionary prism. Earth & Planet Sci Lett 109:451–462.
Yau Y-C, Peacor DR, McDowell SD. 1987. Smectite-to-illite reactions in Salton Sea shales: A transmission and analytical electron microscopy study. J Sed Pet 57:335–342.

(Received 15 March 1995; accepted 1 August 1995; Ms. 2637)